

Auxiliary materials for

Tomography of the 2011 Iwaki earthquake (M 7.0) and Fukushima nuclear power plant area

Ping Tong^{1,2}, Dapeng Zhao¹ and Dinghui Yang²

[1] {Department of Geophysics, Tohoku University, Sendai 980-8578, Japan}

[2] {Department of Mathematical Sciences, Tsinghua University, Beijing, China}

Correspondence to: P. Tong (tongping85@gmail.com)

D. Zhao (zhao@aob.gp.tohoku.ac.jp)

1 Resolution tests

We conducted checkerboard resolution tests to confirm the reliability of the obtained tomographic images. To make a checkerboard, we assigned alternative positive and negative velocity anomalies of 6% to all the 3-D grid nodes. Random errors with a standard deviation of 0.1 s were added to the synthetic arrival times calculated for the checkerboard model to account for the picking errors existing in the real data.

Figs. S1 and S2 show the finite-frequency results of the checkerboard tests at four layers in the crust under the area where the 2011 Iwaki earthquake occurred and the Fukushima nuclear power plant (FNPP) is located for the Vp and Vs structures, while Figs. S3 and S4 show the finite-frequency results at four layers in the upper mantle beneath the whole study area. The corresponding test results with the ray tomography method (Zhao et al., 1992) are demonstrated in Figs. S5-S8. Although the resolution is lower at 12.0 km depth, the results of resolution tests indicate that the two tomographic methods can well resolve

the heterogeneities in the Iwaki earthquake and FNPP area. To further demonstrate the recovery ability of the tomographic methods, we adopted the structural similarity (SSIM) index (Tong et al., 2011) to quantitatively measure the recovery rate of synthetic test with respect to the checkerboard model. For both the finite-frequency and ray tomography methods, Table S1 shows the SSIM indices between the input checkerboard model and the inversion results at different depths. Each index in this table corresponds to one subfigure in Figs. S1-S8. The SSIM indices indicate that the data set used in this study guarantees satisfactory recovery rates for both tomographic methods.

2 Ray and finite-frequency tomographic images

The finite-frequency results of the crustal Vp and Vs structures at four representative layers in the Iwaki earthquake and FNPP area are shown in Figs. S9 and S10. The corresponding results of ray tomography are demonstrated in Figs. S11 and S12. Strong lateral heterogeneities are revealed in the study area (Figs. S9-S12). The 2011 Iwaki mainshock (M 7.0) and its large aftershocks (M > 5.0) are located in a boundary zone with strong variations in seismic velocities. Low-velocity (low-V) anomalies are noticeable in the upper crust in and around FNPP.

Comparing Figs. S9-S10 with Figs. S11-S12, we can see that the finite-frequency and ray tomography methods have generated nearly the same velocity images. The only difference is that the finite-frequency results exhibit slightly higher amplitudes of velocity perturbations, which was also found by the previous studies (e.g., Gautier et al., 2008; Tong et al., 2011). The consistency of the tomographic results generated by the two

different methods is quantitatively verified by the SSIM indices between the two tomographic models at different depths (Table S2).

Figs. S13 and S14 display the cross-sectional views of tomographic images along different profiles with the ray tomography method. The corresponding finite-frequency images are shown in Figs. 3 and 4. Similar to the map views (Figs. 9-12), the overall patterns of the cross-sectional views generated by the finite-frequency and ray tomography methods are nearly the same.

Auxiliary References

Gautier, S., Nolet, G., and Virieux, J.: Finite-frequency tomography in a crustal environment: Application to the western part of the Gulf of Corinth, *Geophys. Prospect.*, 56, 493-503, 2008.

Tong, P., Zhao, D., and Yang, D.: Tomography of the 1995 Kobe earthquake area: comparison of finite-frequency and ray approaches, *Geophys. J. Int.*, 187, 278-302, 2011.

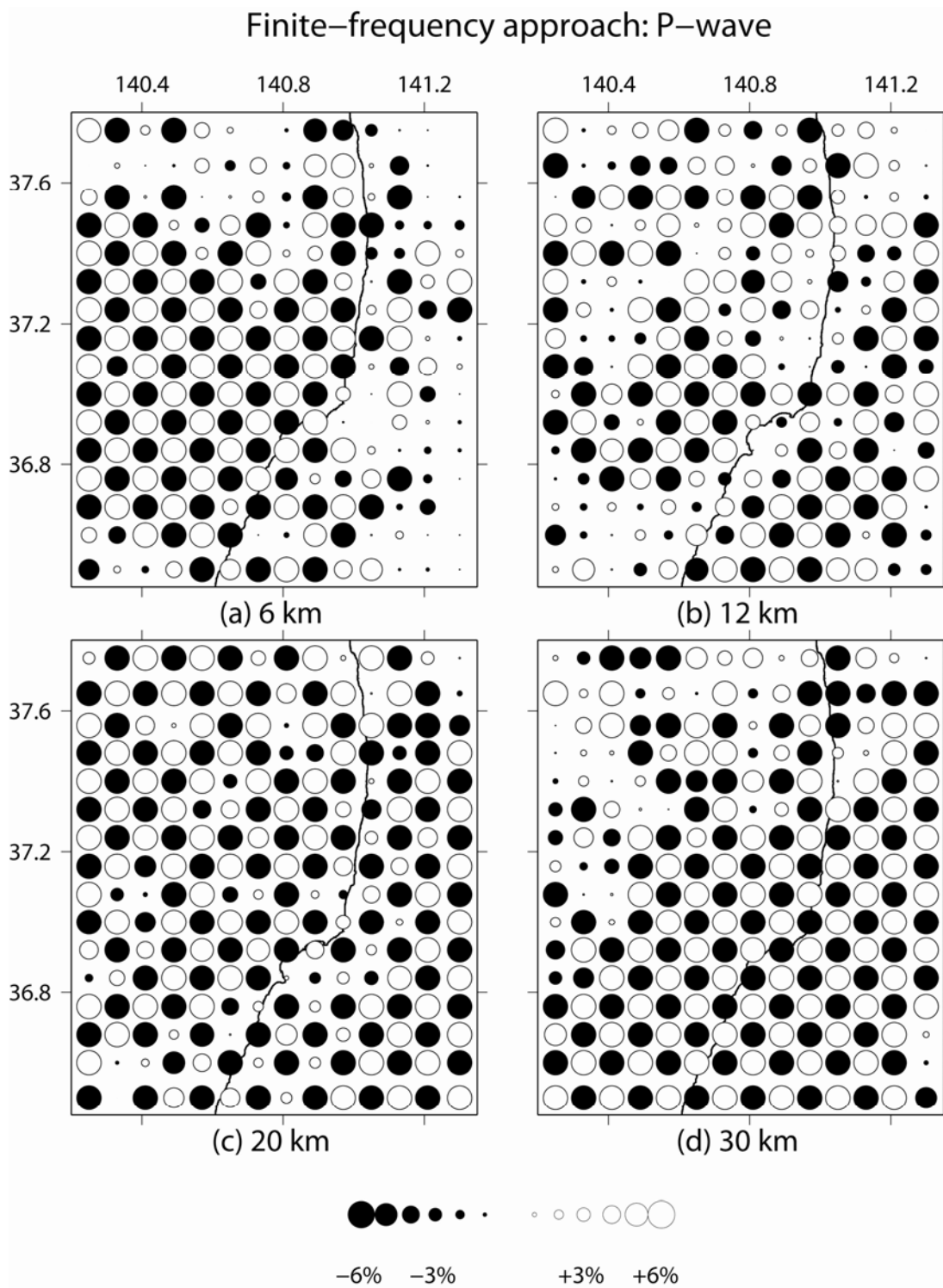
Zhao, D., Hasegawa, A., and Horiuchi, S.: Tomographic imaging of P and S wave velocity structure beneath northeastern Japan, *J. Geophys. Res.*, 97, 19,909-19,928, 1992.

Table S1: Structural similarity (SSIM) indices between the checkerboard model and the inversion result at different depths for P-wave and S-wave velocity structures. In the crust (at the depths of 6.0, 12.0, 20.0 and 30.0 km), the SSIM indices are calculated in the Iwaki earthquake and Fukushima nuclear power plant area; while in the upper mantle (at the depths of 40.0, 60.0, 90.0 and 120.0 km), they are calculated for the whole study region. The inversion results are obtained by using finite-frequency tomography (FFT) or ray approach.

Depth (km)	6.0	12.0	20.0	30.0	40.0	60.0	90.0	120.0
FFT: P-wave	0.8323	0.7146	0.9634	0.9614	0.9109	0.9478	0.9211	0.7961
Ray: P-wave	0.8664	0.6969	0.8859	0.9728	0.9462	0.9558	0.9347	0.8156
FFT: S-wave	0.8593	0.7641	0.9589	0.9663	0.9400	0.9693	0.9462	0.8367
Ray: S-wave	0.8480	0.6859	0.8836	0.9578	0.9385	0.9639	0.9445	0.8289

Table S2: Structural similarity (SSIM) indices between the finite-frequency and ray tomography results at different depths under the whole study area.

Depth (km)	6.0	12.0	20.0	30.0	40.0	60.0	90.0	120.0
P-wave	0.9628	0.9642	0.9555	0.9908	0.9331	0.9661	0.9847	0.9926
S-wave	0.9745	0.9696	0.9742	0.9868	0.9682	0.9758	0.9937	0.9970

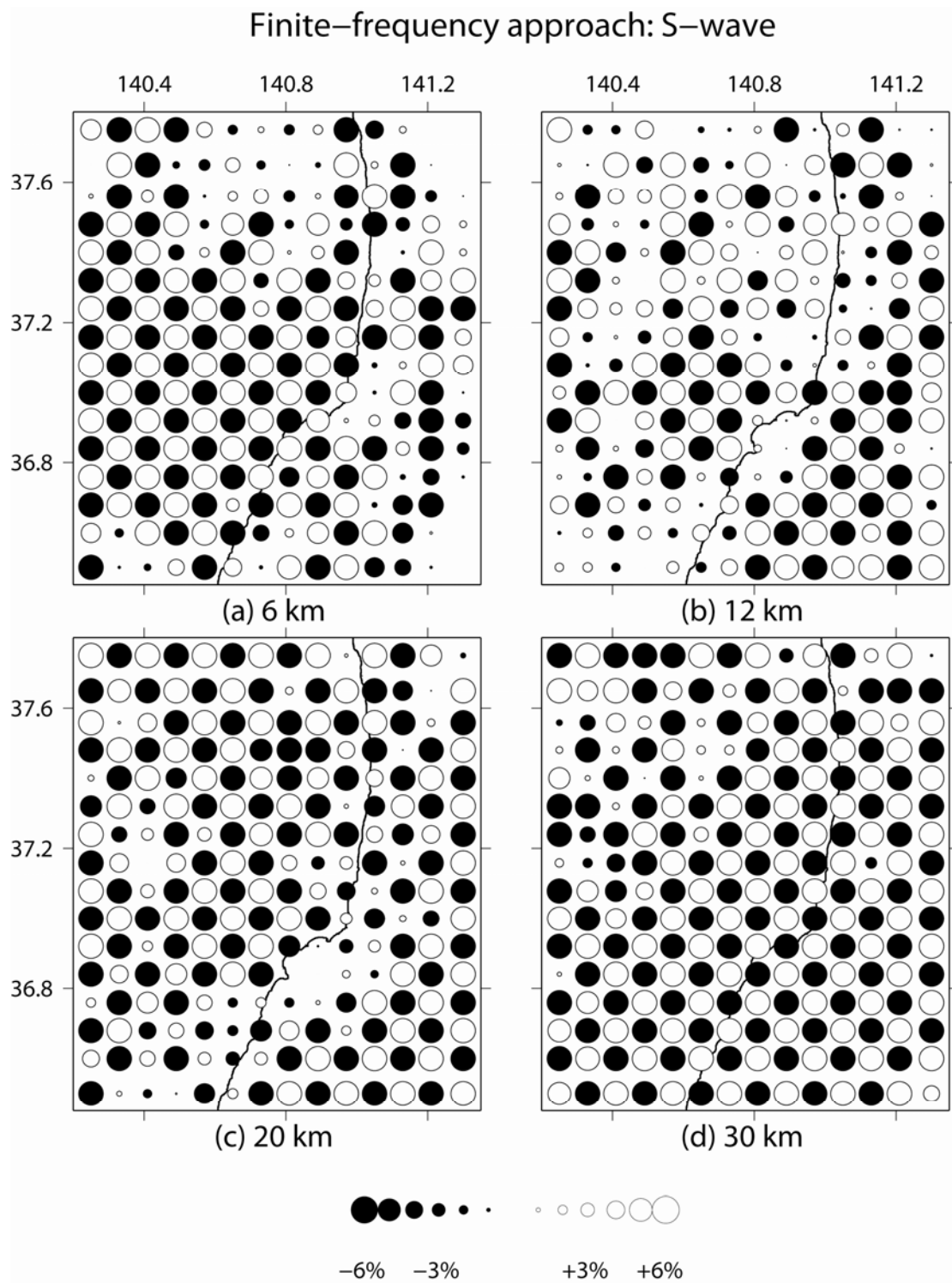


85

86 Figure S1. Finite-frequency results of a checkerboard resolution test for V_p structure at

87 four representative depth layers in the crust under the Iwaki earthquake and the

88 Fukushima nuclear power plant area.

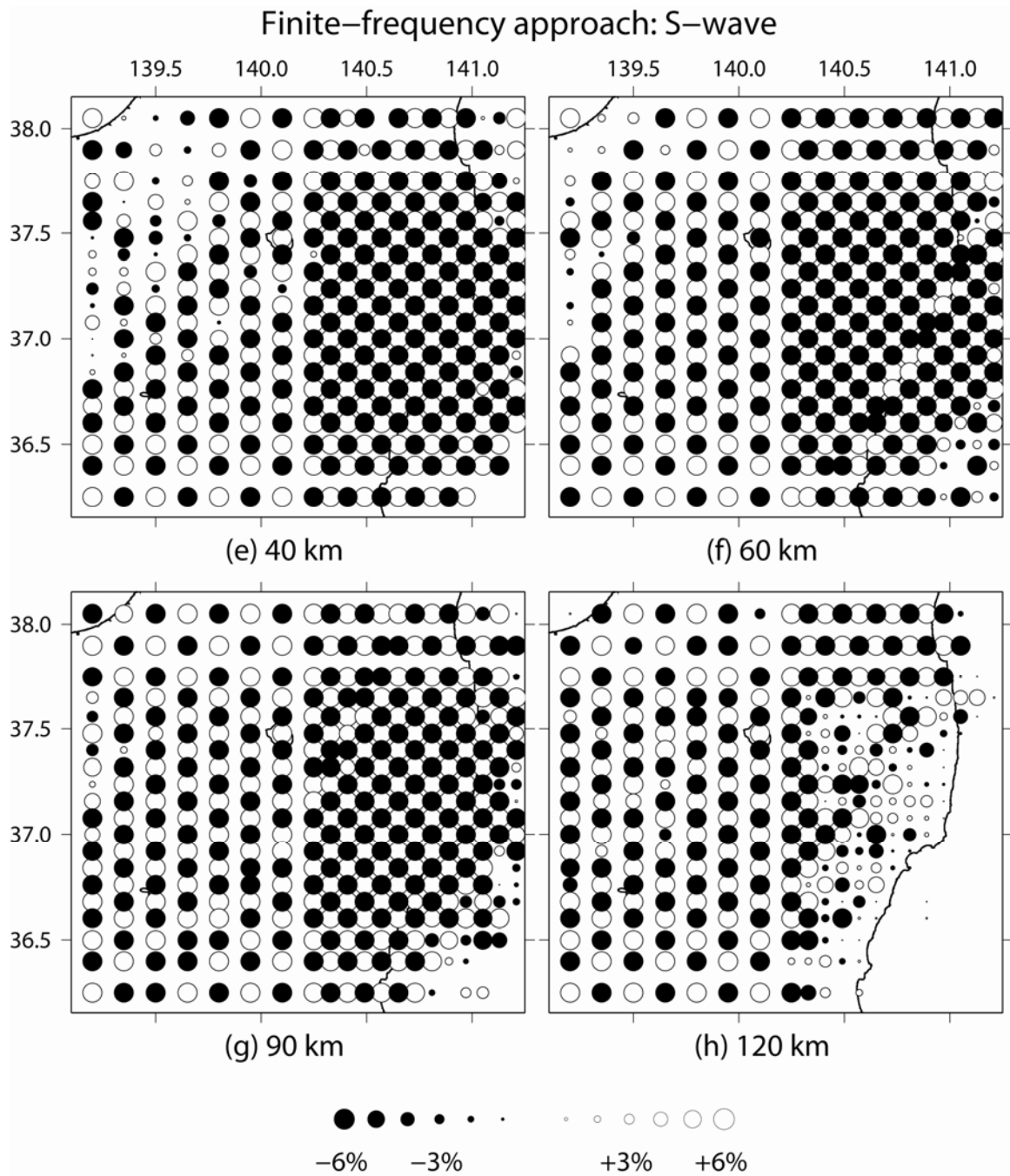


89

90

91 Figure S2. The same as Fig. S1 but for Vs structure.

92

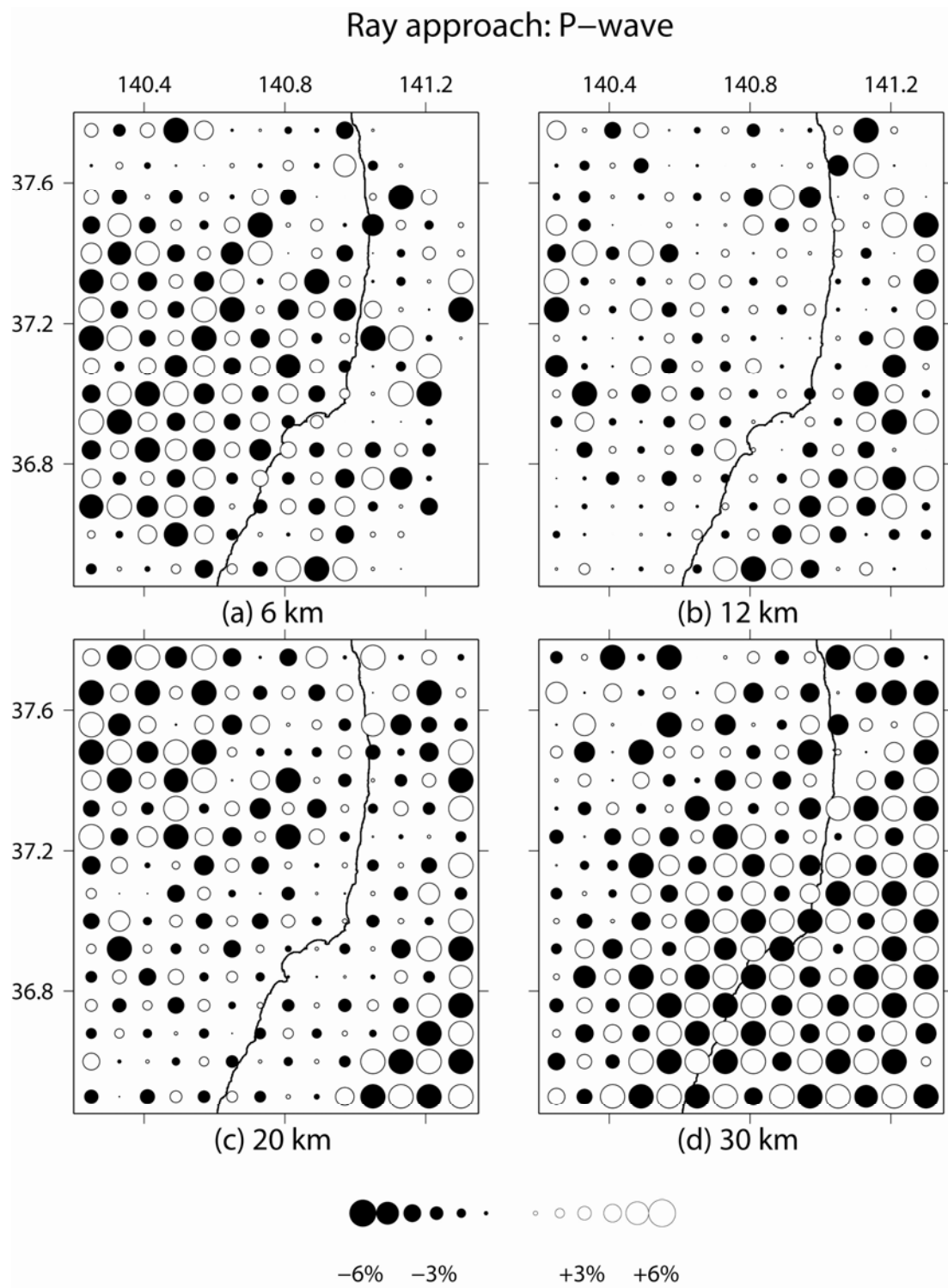


99

100

101 Figure S4. The same as Fig. S3 but for Vs structure.

102

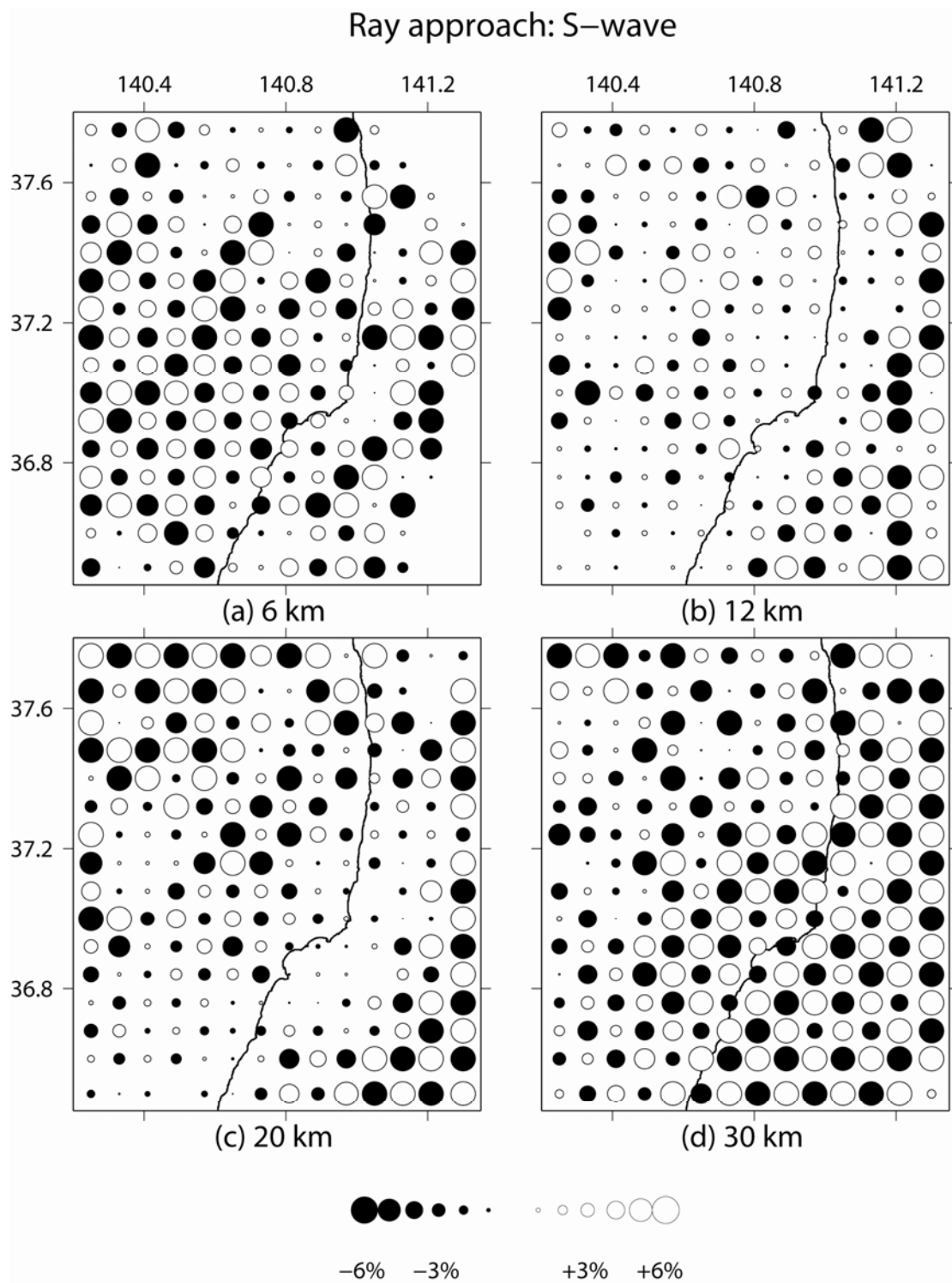


103

104 Figure S5. Ray approach results of a checkerboard resolution test for Vp structure at four

105 representative depth layers in the crust under the Iwaki earthquake and the Fukushima

106 nuclear power plant area.



107

108 Figure S6. The same as Fig. S5 but for Vs structure.

109

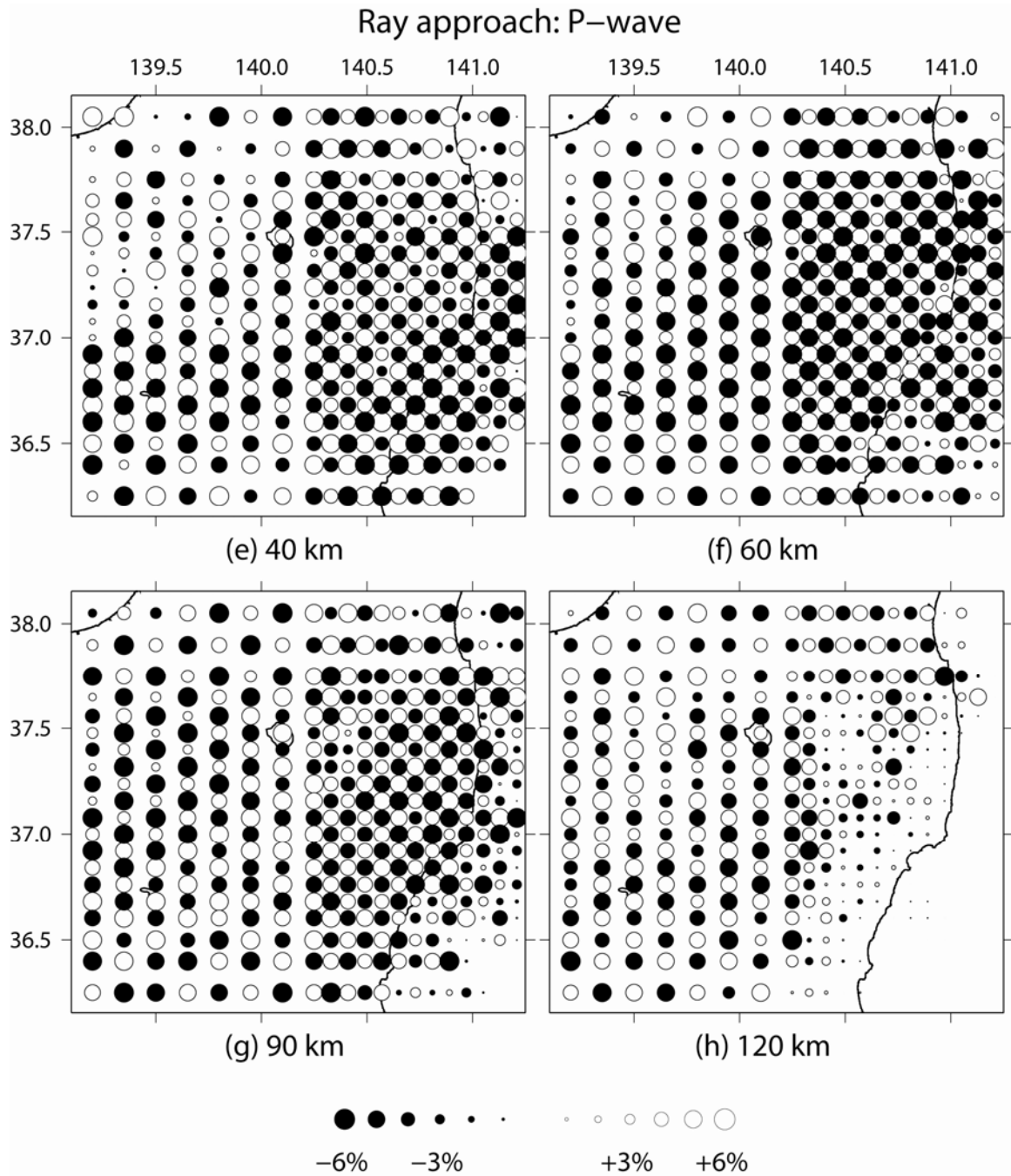


Figure S7. Ray approach results of a checkerboard resolution test for V_p structure at four representative depth layers in the upper mantle under the whole study area.

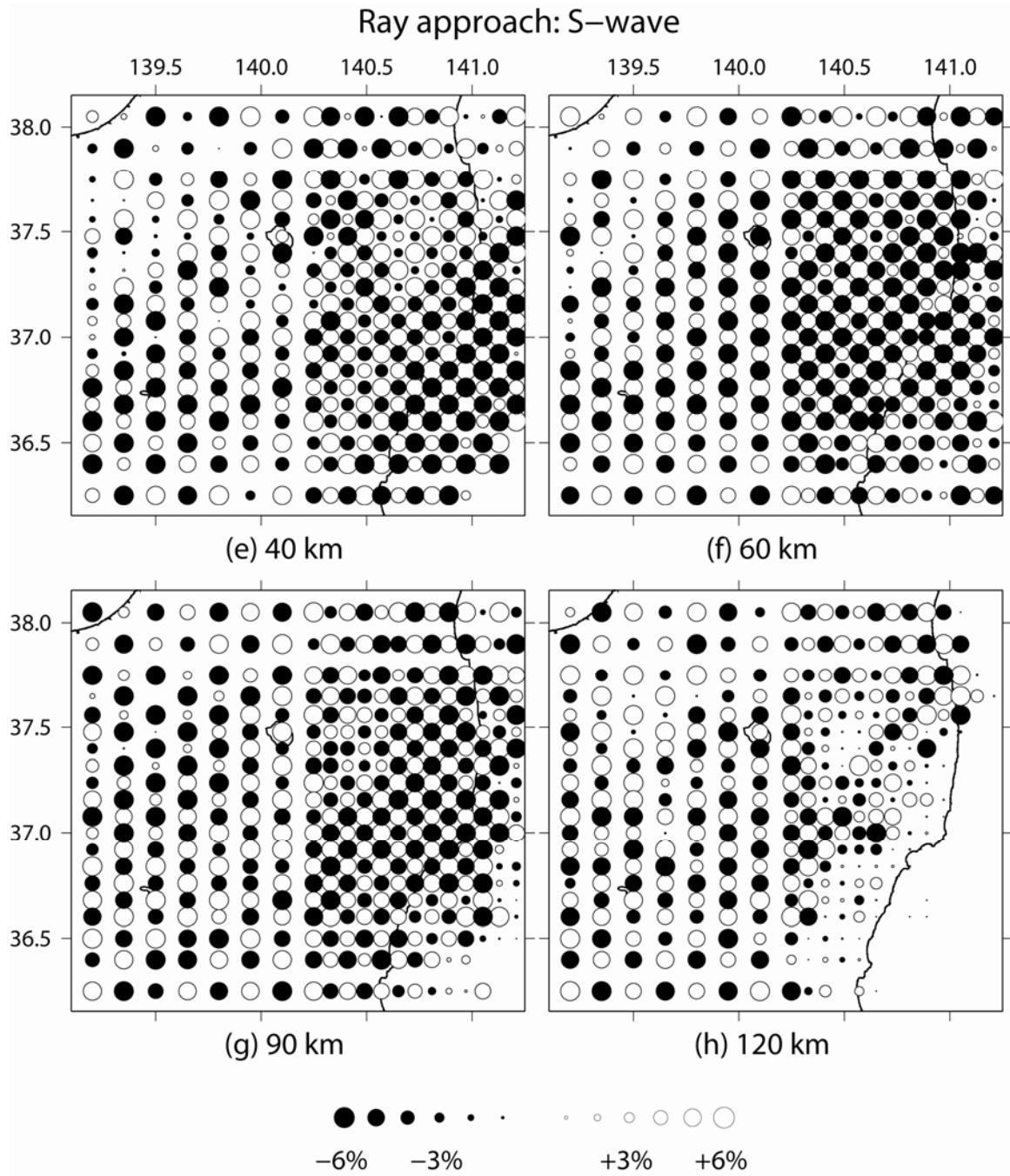
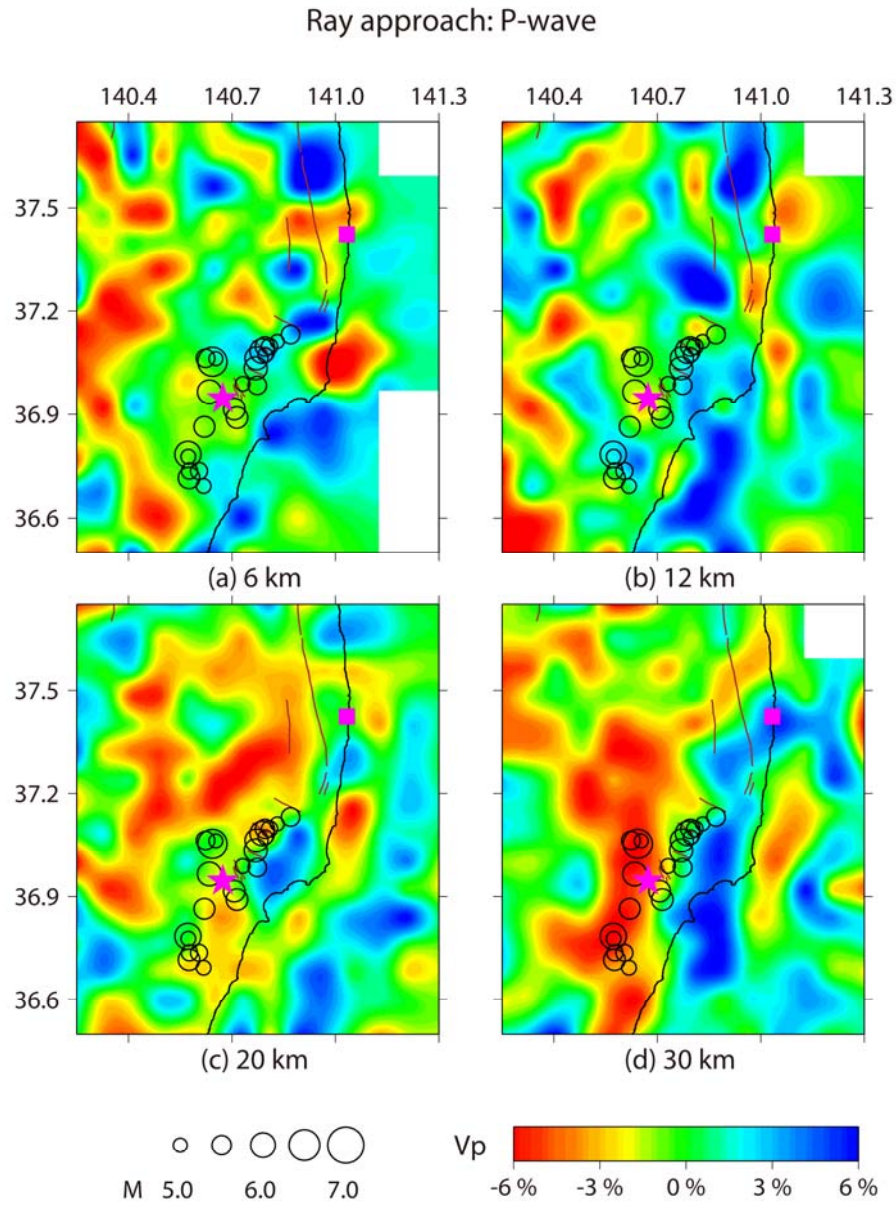


Figure S8. The same as Fig. S7 but for Vs structure.



122

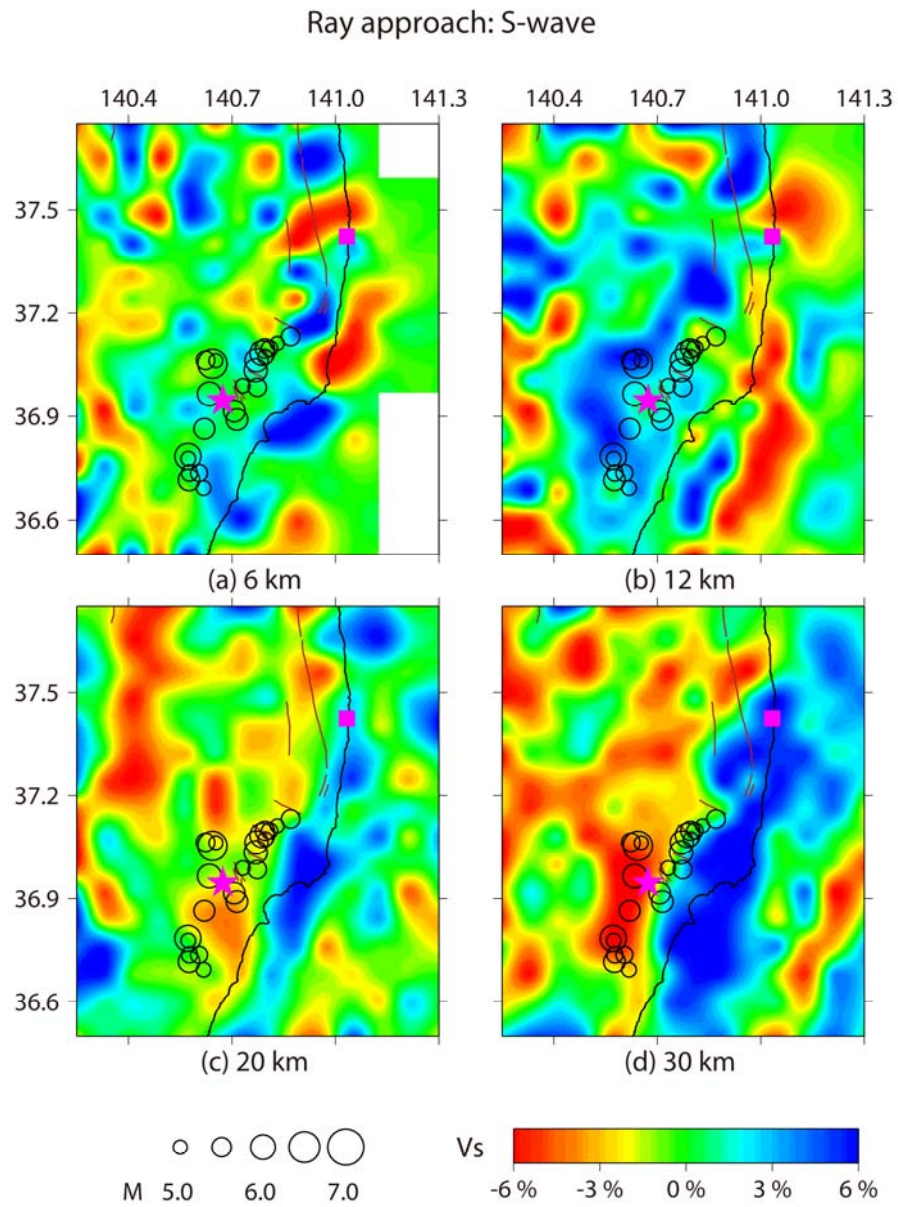
123 Figure S9. Map views of the P-wave tomography with the ray approach in the crust under

124 the Iwaki earthquake and Fukushima nuclear power plant area. The layer depth is shown

125 below each map. Red and blue colors denote low and high velocities, respectively. The

126 velocity perturbation (in %) scale is shown at the bottom. The brown lines denote the

127 active faults.



128

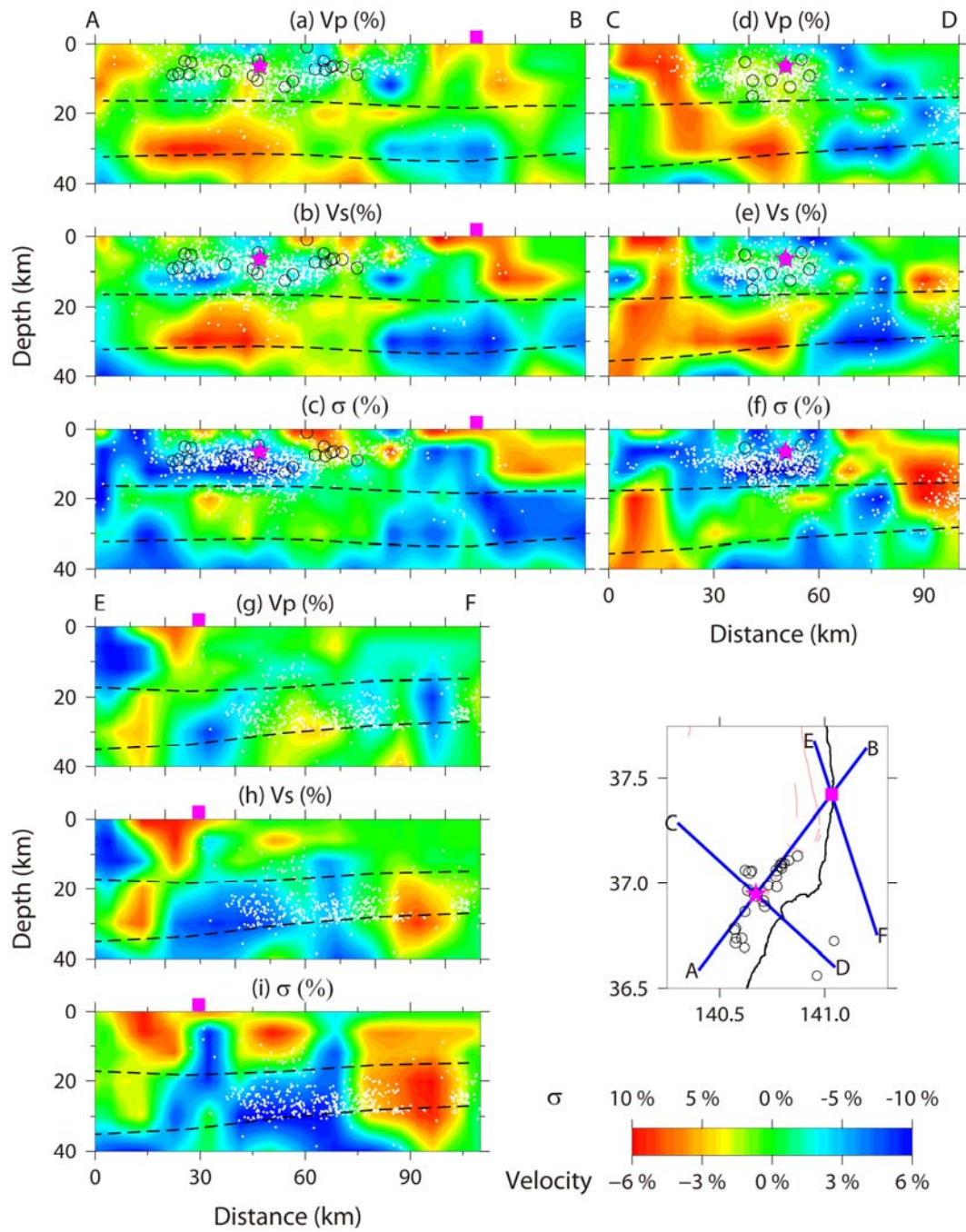
129

130 Figure S10. The same as Fig. S9 but for Vs structure.

131

132

133



134

135

136 Figure S11. Vertical cross-sections of P-wave velocity, S-wave velocity, and Poisson's

137 ratio images obtained with the ray tomography along the lines AB (a-c), CD (d-f) and EF

138 (g-i) as shown on the inset map. The vertical exaggeration is 1:1. Small white dots denote
139 the events during 11 March 2011 to 27 October 2011, which are located within 8-km
140 width along each line. The star symbol denotes the hypocenter of the Iwaki mainshock
141 (M 7.0) with a focal depth of 6.4 km, while the open circles show the Iwaki aftershocks
142 (M > 5.0). The square symbol represents the Fukushima nuclear power plant. The Conrad
143 and the Moho discontinuities are shown in dashed lines. This figure is the same as Fig. 3
144 but obtained with ray tomography.

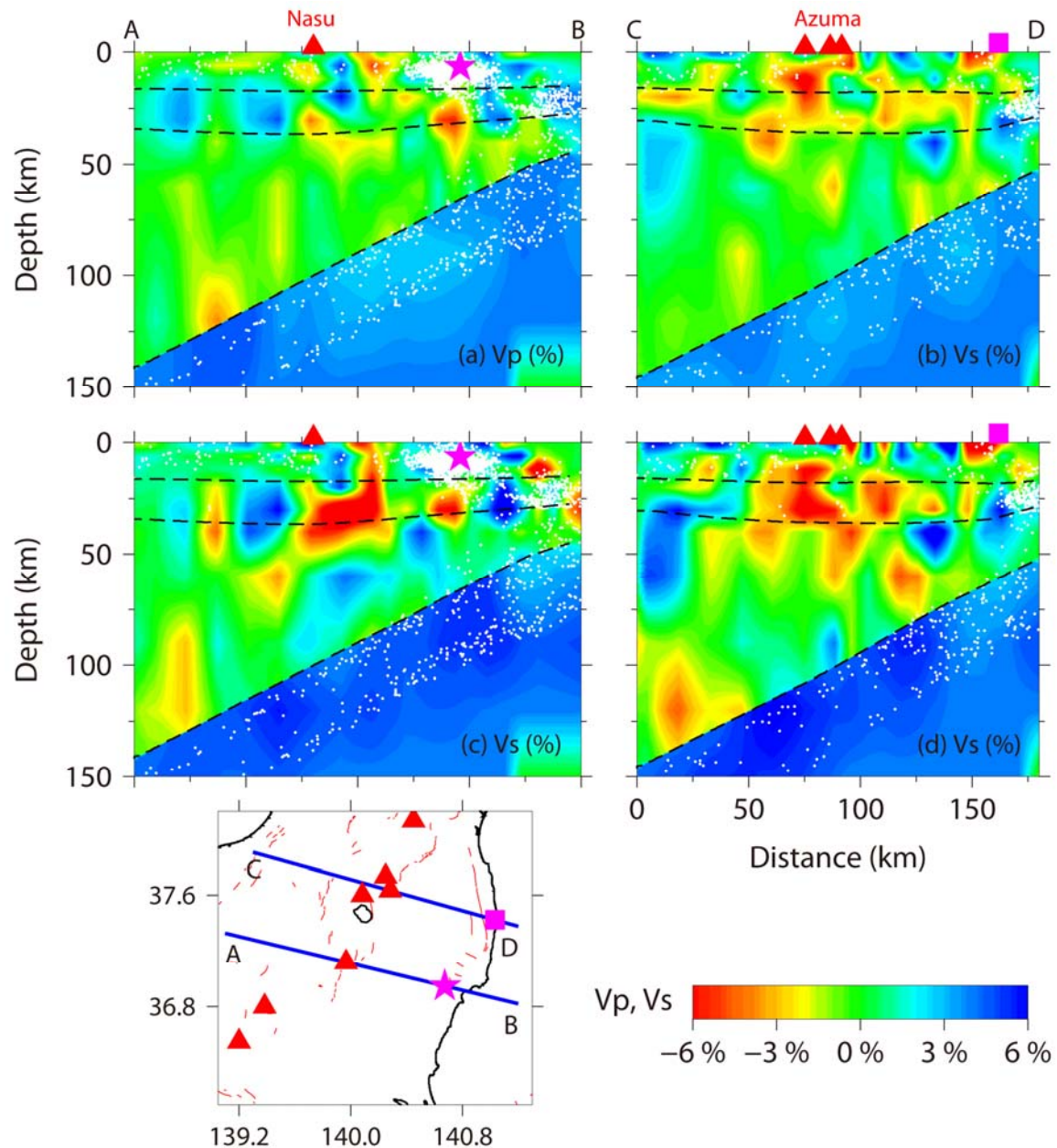
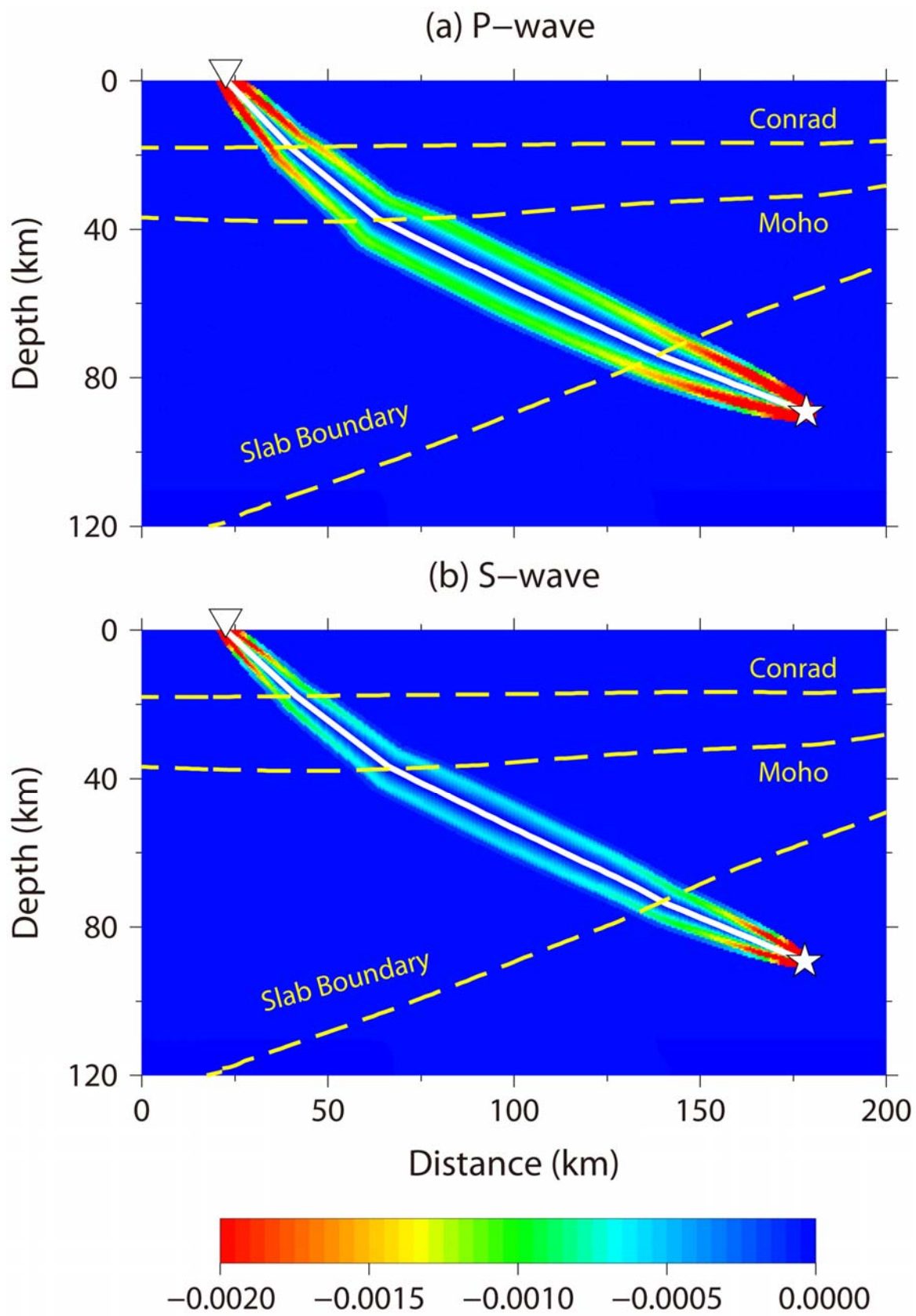


Figure S12. Vertical cross-sections of (a, b) P-wave and (c, d) S-wave velocity images in the depth range of 0-150 km along the lines AB and CD as shown on the inset map. The vertical exaggeration is 1:1. Small white dots denote the events during 3 June 2002 to 27 October 2011, which are located within a 20-km width along each line. The star and square symbols denote the hypocenter of the Iwaki mainshock (M 7.0) and the

152 Fukushima nuclear power plant, respectively. The triangle symbol represents the active
153 volcanoes. The three dashed lines denote the Conrad and Moho discontinuities and the
154 upper boundary of the subducting Pacific slab. This figure is the same as Fig. 4 but
155 obtained with ray tomography.



157

158 Figure S13. Examples of the finite-frequency traveltime sensitivity kernels with a
159 dominant frequency of 4.0 Hz in a 1-D velocity model for (a) P-wave and (b) S-wave.
160 The earthquake represented by the star is located within the subducted Pacific slab. The
161 inverse triangle denotes the source and receiver. The curved white lines represent the
162 geometrical ray paths. The yellow lines show the Conrad and Moho discontinuities and
163 the upper boundary of the subducted Pacific slab.